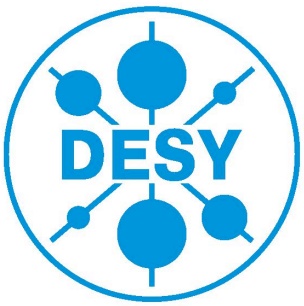


# Global Fit of the Strong Coupling Constant $\alpha_s(M_Z)$ Using Inclusive Jet Cross-Section Data From HERA, LHC and Tevatron Experiments

Kristian Bjørke[a*]

Supervisors: Daniel Britzger[b], Hayk Pirumov[b]

[a] University of Sussex, United Kingdom [b] DESY, Hamburg, Germany

September 6, 2015

**Abstract**

We have used inclusive jet cross-section data from HERA, LHC and Tevatron publications to do a global fit of the fundamental QCD parameter, the strong coupling constant $\alpha_s(M_Z)$. Bin-to-bin correlations of specific experimental uncertainties and between different experimental data sets have been considered. Several theoretical uncertainties have been studied. The result for the fit is $\alpha_s(M_z) = 0.12055 \pm 0.00055\ (\text{exp.})\ ^{+0.0028}_{-0.0038}\ (\text{th.})$, which is cosistent with the current world average of $\alpha_s(M_Z) = 0.1185 \pm 0.0006$ [3].

*kbjorke@gmail.com

# Contents

# 1 Introduction

The goal of this project is to make a global fit of the fundamental QCD parameter, the strong coupling constant $\alpha_s$, which if we assume fixed masses is the only free parameter of QCD. To do this we will be using data taken from detectors at the HERA, LHC and Tevatron experiments.

The work will consist of choosing a method for the fit, assembling the data with uncertainties and correlations and theory predictions, performing the fit, evaluating the uncertainties on the fit, and discuss the final result and compare it to the current world average for $\alpha_s$, see Figure 1. The world average is based on averaging the five pre-averaged values in Figure 1, which are based on full NNLO QCD predictions and are published in peer-reviewed journals at the time of the averaging.

This report starts with a theory section that introduces Quantum Chromodynamics and what kind of interactions we will be studying. Then we present the method we use for the fit. After this the data from different experiments is discuss along with correlations. We also here present the theory predictions we will base our fit on. Then we will present our results along with a study of the quality of the fit and its uncertainties. Last, in the conclusion, we will summarize our results.

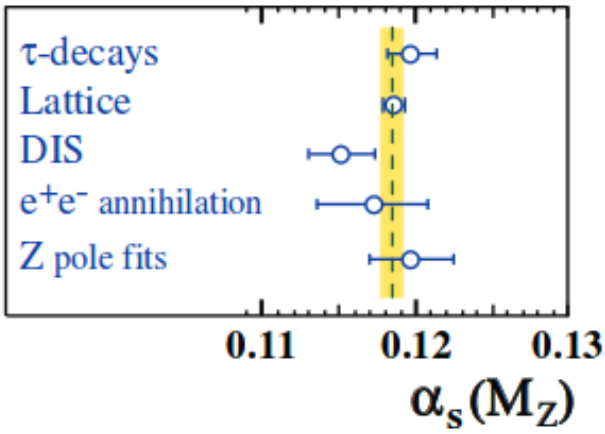


Figure 1: Summary of values of $\alpha_s(M_Z)$ for subclasses of measurements. World average is indicated by dashed line and yellow band. [3]

# 2 Theory

## 2.1 Quantum Chromodynamics

Quantum Chromodynamics[2, 2] (QCD) is the component of the Standard Model that describes the interactions between colored quarks and gluons wich is mediated by the strong force. QCD is described by its Lagrangian:

$$\mathcal{L}_{QCD} = \sum_q \bar{\psi}_{q,a}(i\gamma^\mu \partial_\mu \delta_{ab} - g_s \gamma^\mu t^C_{ab} \mathcal{A}^C_\mu - m_q \delta_{ab})\psi_{q,b} - \frac{1}{4} F^A_{\mu\nu} F^{\mu\nu}_A \ , \tag{1}$$

where $\psi_{q,a}$ represents colored quarks, $\mathcal{A}^C_\mu$ represents the colored gluons, and the coupling constant $g_s$ determines the strength of their interaction. We see from the Langrangian that the quark masses, $m_q$, and the strong coupling, $g_s$ ($\alpha_s = \frac{g_s^2}{4\pi}$), are the fundamental parameters of QCD.

The theory of QCD exhibits ultra-violet divergencies when calculating diagrams including loop corrections. In order to obtain finite solutions for physical obervables we have to preform regularization. This process includes the introduction of a new scale called the renormalization scale, $\mu_r$, which makes any physical quantity as the coupling $\alpha_s(\mu_r)$ a function of the scale. A physical quantity $\mathcal{R}$ should not depend on a arbitrary choice of $\mu_r$, so we introduce the renormalized group equation (RGE)

$$\mu_r^2 \frac{\mathrm{d}}{\mathrm{d}\mu_r^2} \mathcal{R}(Q^2/\mu_r^2, \alpha_s) = 0 \ , \tag{2}$$

which leads to the following equation for the coupling

$$\mu_r^2 \frac{\mathrm{d}\alpha_s}{\mathrm{d}\mu_r^2} = \beta(\alpha_s) \tag{3}$$

In 1-loop approximation there exists a solution to (3)

$$\alpha_s(\mu_r, \alpha_s(M_Z)) = \frac{\alpha_s(M_Z)}{1 + \alpha_s(M_Z)\beta_0 \ln \mu_r^2/M_Z^2} \ , \tag{4}$$

where $M_Z$ is the mass of the $Z^0$ boson. This equation gives rise to the running of the strong coupling, see Figure 2.

Also we need to introduce a factorization scale, $\mu_f$, which is a scale to separate short-distance interactions (hard processes of the partons) from long-distance interactions. This is done so that perturbative QCD (pQCD) does not break down.

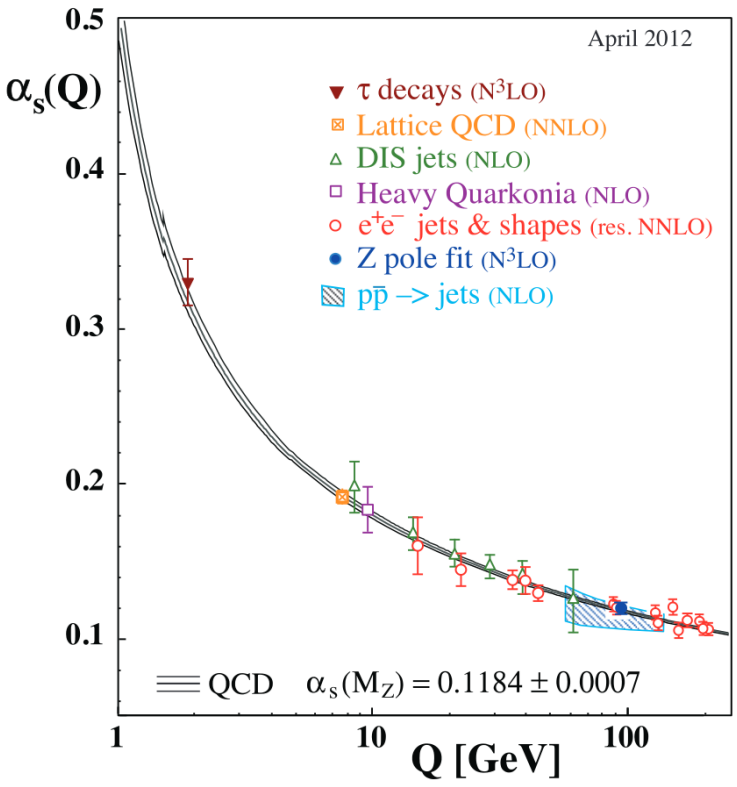


Figure 2: Illustration of the running coupling $\alpha_s(\mu_r)$ along with several determinations of the $\alpha_s(M_Z)$ at the scale of their determination. [3]

## 2.2 Inclusive jet production

In order to determine the strong coupling constant we will be using measured cross sections of inclusive jet production from hadron-hadron (p-p,p-$\bar{\text{p}}$) colliders and lepton-hadron (e-p) colliders.

In the case of hadron-handron collisions we can write the jet production cross section as

$$\sigma_{hh} = \sum_n \alpha_s^{2+n}(\mu_r) \otimes f_1(x_1, \mu_f) \otimes f_2(x_2, \mu_f) \otimes \hat{\sigma}(\mu_r, \mu_f) \cdot c_{NP} \cdot c_{EW} \ , \tag{5}$$

where the leading order contribution is of order $\Omega(\alpha_s^2)$. Similarily one can write the jet production cross section for deep inelastic scattering (DIS) as

$$\sigma_{DIS} = \sum_n \alpha_s^{1+n}(\mu_r) \otimes f_1(x_1, \mu_f) \otimes \hat{\sigma}(\mu_r, \mu_f) \cdot c_{NP} \cdot c_{EW} \ , \tag{6}$$

where the LO contribution is of order $\Omega(\alpha_s)$.

In equations (5) and (6) we have included up to next-to-leading order $n = 1$ processes. $f_i(x_i, \mu_f, \hat{\alpha_s})$ represents the parton distribution functions (PDFs), $c_{NP}$ and $c_{EW}$ are the

non perturbative and the electroweak corrections respectivly.

# 3 Method of fit

This section adresses the method we will be using for the fit.

## 3.1 Least square fitting

The fit will be done by using the method of least squares, as described in [4]. In the least square method we want to minimize the $\chi^2$ value, which is in it's simples form given as

$$\chi^2(\boldsymbol{\theta}) = \sum_{i=1}^{N} \frac{(y_i - \mu(x_i;\boldsymbol{\theta}))^2}{\sigma_i^2} \ , \tag{7}$$

where $\boldsymbol{\theta}$ are the parameters we want to set, $y_i$ independent measurements at $x_i$ with uncertainty $\sigma_i$, and $\mu(x_i;\boldsymbol{\theta})$ are the theoretical predictions.

Often the measurements are not independet, then we need to introduce the covariance matrix $V_{ij} + \mathrm{cov}[y_i, y_j]$ and the new $\chi^2$ definition of

$$\chi^2(\boldsymbol{\theta}) = (\boldsymbol{y} - \boldsymbol{\mu}(\boldsymbol{\theta}))^T V^{-1} (\boldsymbol{y} - \boldsymbol{\mu}(\boldsymbol{\theta})) \ , \tag{8}$$

where $\boldsymbol{y}_i = (y_i, \ldots, y_N)$ is a vector of the measurements, and $\boldsymbol{\mu}(\boldsymbol{\theta})$ the corresponding vector of theory predictions.

For our fit we are using the lognormal definition of the $\chi^2$ which looks like

$$\chi^2(\boldsymbol{\theta}) = (\log(\boldsymbol{y}) - \log(\boldsymbol{\mu}(\boldsymbol{\theta})))^T V^{-1} (\log(\boldsymbol{y}) - \log(\boldsymbol{\mu}(\boldsymbol{\theta}))) \ , \tag{9}$$

where the matrix $V$ contains the uncertainties of the measurements and the correlations between measurements.

## 3.2 Alpos code

For the fitting we have used the Alpos[1] program, which is an C++ based object-oriented data to theory comparison and fitting framework. The alpos program can use different sets of data and theory predictions, analysis sets and fitting parameters, which makes is well suited for a global fit of the strong coupling $\alpha_s(M_Z)$ based on data from different experiments.

Through the Alpos steering file one can specifiy what data to include in the fit, the theory sets, the fitting method and tasks to be performed on these inputs. The important tasks

[1] https://ekptrac.physik.uni-karlsruhe.de/svn/Alpos/trunk

to mention is the StatAnalysis task, which returns information about the statistics of the fit and the $\chi^2$ value, the AFitter task, which preforms the actual minimization of the $\chi^2$ and returns the fitted parameter with uncertainty.

In addition to this we have during this project implemented the Chi2Scan task, which returns $\chi^2$ parabolas for the fits (5.2), and the PDFUncer task, which generates a histogram which is used to analyses the uncertainty on the PDF set used for the fit (5.3).

# 4 Data used for fit

## 4.1 Inclusive jet cross-section data

For the fit we have used inclusive jet data from the HERA experiment at DESY, the LHC experiment at CERN and the Tevatron experiment at Ferimilab. A compilation of some fo the data used is shown in Figure 3. An overview of the datafiles used and their respective publications are included in Table 1. More information about each data set is presented in Tabel 9 at the end of the report. All datafiles contains cross sections for inclusive jet production for different $p_T$ regions and different rapidity regions, for $pp$ collisions, and $Q^2$ regions for DIS, respectivly.

Table 1: Overview of the datafiles used for the fitting, with a reference to the publication of the data. The datafiles from HERA, LHC and Tevatron experiments are separated by horisontal lines. (PRL: Physical Review Letters.)

| **AposName** | **SteerFile** | **References** |
|---|---|---|
| H1-HERAI-LowQ2-99/00-InclJets | H1_InclJets_LowQ2_99-00-alpos.dat | [10] |
| H1-HERAI-HighQ2-99/00-InclJets | H1_InclJets_HighQ2_99-00-alpos.dat | [11] |
| ZEUS-HERAI-HighQ2-96/97-InclJets | ZEUS_InclJets_HighQ2_96-97-alpos.dat | [12] |
| ZEUS-HERAI-HighQ2-98/00-InclJets | ZEUS_InclJets_HighQ2_98-00-alpos.dat | [13] |
| H1HeraII-NormInclJets | normIncl-alpos.dat | [14] |
| CDF-InclJet-RunII | CDF-InclJets-2008-alpos.dat | [15] |
| D0-InclJet-RunII | D0-InclJets-2009-alpos.dat | [16] |
| CMS-InclJets-7TeV-RunI | CMS_IncJets2011_QCD_11_004-alpos.dat | [17] |
| ATLAS_InclJets2010_7TeV_R06 | ATLAS_InclJets2010_R06.dat | [18] |
| ATLAS_InclJets2011_2.76_R06 | ATLAS_InclJets2011_2p76_R06.dat | [19] |
| ATLAS_InclJets_7TeV_2011 | ATLAS_IncJets2011_R06.dat | [20] |

h!

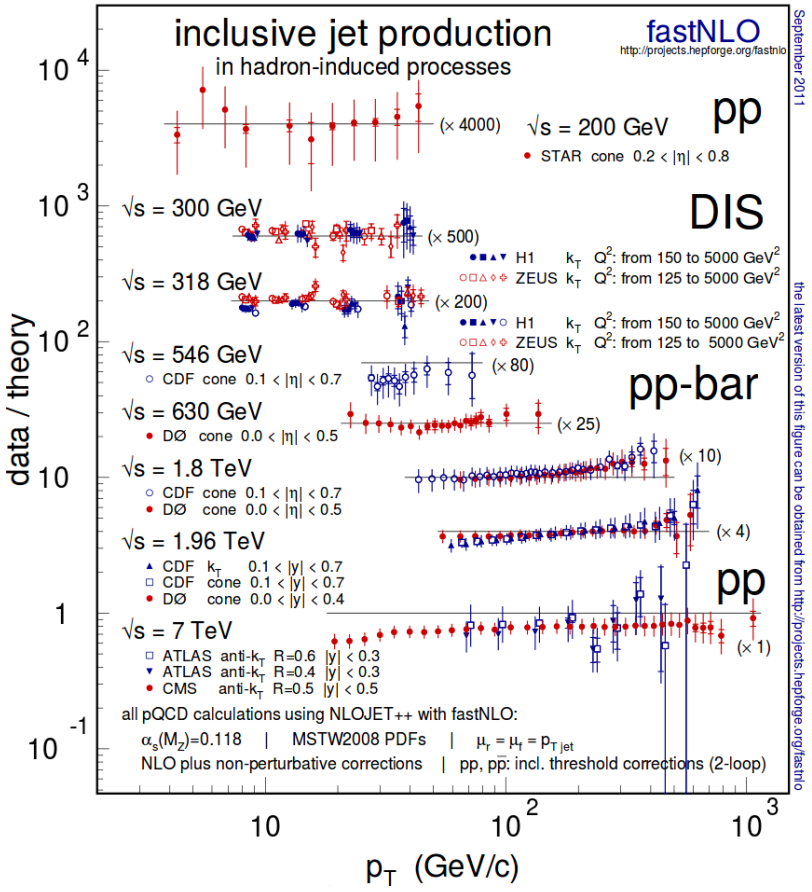


Figure 3: A compilation of inclusive jet cross section measurements, where most of the data we are using is included.

### 4.1.1 The HERA collider and its experiments

The HERA (Hadron-Elektron-Ringanlage) was a particle accelerator at DESY in Hamburg, Germany. It was used for colliding electron or positrons agains protons at center of mass energies of 318 GeV and 300 GeV. HERA was in operation from 1992 until 2007. In the HERA accelerator there were the four experiments H1, ZEUS, HERMES and HERA-B. In this study we will use data from the H1 and ZEUS experiments.

### 4.1.2 The LHC collider and its experiments

The LHC (Large Hadron Collider) is the world largest circular particle accelerator at CERN in Switzerland. It is an proton proton collider with a design center-of-mass energy of 14 TeV The LHC delivers colissions to the four major experiments called ATLAS, ALICE, CMS and LHCb. In this study we have used data from the ATLAS and CMS experiments, taken at center of mass energies of 2.76 and 7 TeV.

### 4.1.3 The Tevatron collider and its experiments

The Tevatron was a particle accelerator at Fermilab in the USA. It was used to collide protons and antiprotons of energies up to 980 GeV. The Tevatron accelerator was in operation from 1987 until 2011. At Tevatron there where two detector experiments called CDF and D0. In this study we use data from both of these experiments.

## 4.2 Data correlations

Each experiment handles data acquisition and callibrations differently and therefore the data often comes with a large set of uncertainties which may or may not be correlated with each other. Also different sets of data from the same experiment may also have correlated uncertainties.

In the respective publications for the data the uncertainties and their correlations are typically specified, see for instance Figure 4. We handeled these uncertainties by including them in the Alpos datafiles.

## 4.3 Theory files and PDF sets

Theory files based on the dataset are provided as input to the Alpos code. The files has been privided using fastNLO_2.1.0 [5], and in the datafiles the corresponding theoryfiles is specified. There fastNLO tables are based on calcuilations preforemd with nlojet++.

Another importat part of the theory side of the fit is the parton distribution function (PDF) sets. These are determined using experimental data and theoretical calculations up to next-to-next-to leading (NNLO) order in QCD. There are a variety of PDF set

| Uncertainty source | $\|y\|$ bins | | | | | | | Correlation |
|---|---|---|---|---|---|---|---|---|
| | 0-0.3 | 0.3-0.8 | 0.8-1.2 | 1.2-2.1 | 2.1-2.8 | 2.8-3.6 | 3.6-4.4 | to 7 TeV |
| Trigger efficiency | $u_1$ | $u_1$ | $u_1$ | $u_1$ | $u_1$ | $u_1$ | $u_1$ | N |
| Jet reconstruction eff. | 83 | 83 | 83 | 83 | 84 | 85 | 86 | Y |
| Jet selection eff. | $u_2$ | $u_2$ | $u_2$ | $u_2$ | $u_2$ | $u_2$ | $u_2$ | N |
| JES1: Noise thresholds | 1 | 1 | 2 | 3 | 4 | 5 | 6 | Y |
| JES2: Theory UE | 7 | 7 | 8 | 9 | 10 | 11 | 12 | Y |
| JES3: Theory showering | 13 | 13 | 14 | 15 | 16 | 17 | 18 | Y |
| JES4: Non-closure | 19 | 19 | 20 | 21 | 22 | 23 | 24 | Y |
| JES5: Dead material | 25 | 25 | 26 | 27 | 28 | 29 | 30 | Y |
| JES6: Forward JES generators | 88 | 88 | 88 | 88 | 88 | 88 | 88 | * |
| JES7: $E/p$ response | 32 | 32 | 33 | 34 | 35 | 36 | 37 | Y |
| JES8: $E/p$ selection | 38 | 38 | 39 | 40 | 41 | 42 | 43 | Y |
| JES9: EM + neutrals | 44 | 44 | 45 | 46 | 47 | 48 | 49 | Y |
| JES10: HAD $E$-scale | 50 | 50 | 51 | 52 | 53 | 54 | 55 | Y |
| JES11: High $p_T$ | 56 | 56 | 57 | 58 | 59 | 60 | 61 | Y |
| JES12: $E/p$ bias | 62 | 62 | 63 | 64 | 65 | 66 | 67 | Y |
| JES13: Test-beam bias | 68 | 68 | 69 | 70 | 71 | 72 | 73 | Y |
| JES15: Forward JES detector | 89 | 89 | 89 | 89 | 89 | 89 | 89 | * |
| Jet energy resolution | 76 | 76 | 77 | 78 | 79 | 80 | 81 | Y |
| Jet angle resolution | 82 | 82 | 82 | 82 | 82 | 82 | 82 | Y |
| Unfolding: Closure test | 74 | 74 | 74 | 74 | 74 | 74 | 74 | N |
| Unfolding: Jet matching | 75 | 75 | 75 | 75 | 75 | 75 | 75 | N |
| Luminosity | 87 | 87 | 87 | 87 | 87 | 87 | 87 | N |

Figure 4: Example of how the correlations are given in the publications. Taken from the ATLAS publication of inclusive jet cross-section in $pp$ collisons at $\sqrt{s} = 2.76$ TeV [19] $u_i$ means uncorrolated in $p_T$ and $y$, same number means that the errors are corrolated in $p_T$. The last column specifies corrolation (Y) or not (N) with the ATLAS cross-section measurement at $\sqrt{s} = 7$ TeV [20].

availiable, and in Table 2 we have tested a selection of these for the global fit in order to see how they differ.

For this project we have chosen to use the NNPDF 3.0 [9] NLO PDF set (NNPDF30_nlo_as_0118) extracted with $\alpha_s = 0.118$. While any of the other PDF sets might as well have been used, considering that they give somewhat similar results, the NNPDF 3.0 set is the "recommended default" PDF for MonteCarlo production in ATLAS for Run-II. We choose to use the NLO PDF set, not the NNLO set, because we want to use a PDF set extracted as the same order as the matrix element calculations.

# 5 Results and discussion

## 5.1 $\alpha_s(M_Z)$ fit

Using the methodology, data and settings described before we have preformed the fit for all the datasets (Global) as well as for individual fits for the different experiments (HERA, LHC and Tevatron) and for the specific detectors of the experiments. The

Table 2: Output of global fit using different PDF sets

| **PDF set** | Num | $\boldsymbol{\alpha_s(M_Z)}$ | $\boldsymbol{\sigma}$ | $\frac{\boldsymbol{\chi^2}}{\boldsymbol{ndf}}$ | **Ref.** |
|---|---|---|---|---|---|
| CT14nnlo | 0 | 0.120561 | 0.000556499 | 1.27777 | [6] |
| CT14nlo | 0 | 0.120445 | 0.0005533 | 1.24956 | |
| MMHT2014nlo_asmzlargerange | 0 | 0.120337 | 0.000553051 | 1.25942 | [7] |
| MMHT2014nnlo_asmzlargerange | 0 | 0.121277 | 0.000556427 | 1.29959 | |
| NNPDF23_nlo_as_0118 | 0 | 0.119709 | 0.000550746 | 1.31561 | [8] |
| NNPDF23_nnlo_as_0118 | 0 | 0.120853 | 0.000551983 | 1.35381 | |
| NNPDF30_nlo_as_0118 | 0 | 0.120548 | 0.000553501 | 1.32447 | [9] |
| NNPDF30_nnlo_as_0118 | 0 | 0.121981 | 0.000555767 | 1.34665 | |
| HERAPDF15NLO_ALPHAS | 0 | 0.121302 | 0.000544443 | 2.76028 | N/A |
| HERAPDF15NNLO_ALPHAS | 0 | 0.120463 | 0.000551051 | 1.58361 | |

results, along with uncertainty and the $\chi^2$ per number of degrees of freedom ($ndf$), are included in Table 3

There are a couple of things we can observe from this table. We see that the purpose of doing a global fit is meet by getting a uncertainty of 0.46% for the global fit. This is by itself slightly less than the uncertainty of the world average of 0.51%. Also the actual global fitted value of $\alpha_s(M_Z) = 0.12055$ is larger then 2 standard deviations from the world average of $\alpha_s(M_Z) = 0.1185$.

Table 3: Output for fit of different combinations of datafiles

| **Data set** | $\boldsymbol{\alpha_s(M_Z)}$ | $\boldsymbol{\sigma}$ | $\frac{\boldsymbol{\chi^2}}{\boldsymbol{ndf}}$ |
|---|---|---|---|
| Global | 0.120558 | 0.000553501 | 1.32447 |
| LHC | 0.121024 | 0.0010377 | 1.38853 |
| ATLAS | 0.122826 | 0.0011825 | 1.59723 |
| CMS | 0.11444 | 0.00212944 | 0.849991 |
| HERA | 0.120319 | 0.00067587 | 1.01632 |
| H1 | 0.119541 | 0.000731407 | 1.01599 |
| ZEUS | 0.124914 | 0.00180544 | 0.887674 |
| Tevatron | 0.12095 | 0.00271505 | 1.40428 |
| CDF | 0.120462 | 0.0037013 | 2.09716 |
| D0 | 0.121513 | 0.00399691 | 0.950418 |

Table 4: Output for ATLAS 2011 7 TeV data with changes in correlations

| **Correlation setting** | $\boldsymbol{\alpha_s(M_Z)}$ | $\boldsymbol{\sigma}$ | $\frac{\boldsymbol{\chi^2}}{\boldsymbol{ndf}}$ |
|---|---|---|---|
| All at 1 | 0.123736 | 0.00155587 | 2.12116 |
| Flavour_Response = 0.5 | 0.124515 | 0.00184122 | 0.979584 |
| Flavour_Response = 0 | 0.123895 | 0.00189036 | 0.817352 |
| Flavour = 0.5 | 0.123913 | 0.0015631 | 2.05784 |
| Flavour = 0 | 0.124087 | 0.00156935 | 2.00157 |
| Insitu_LArEMscale = 0.5 | 0.123965 | 0.00210846 | 0.386584 |
| Insitu_LArEMscale = 0 | 0.121679 | 0.00192362 | 0.271787 |

We see that some of the $\frac{\chi^2}{ndf}$ values deviate from the ideal value of $\sim 1$. The reason for this might be that the uncertainties are overestimated or underestimated, or that the bin-to-bin correlations have not been given correctly. To see how this works we performed fits where we have used different correlations setting for a selection of uncertainties, the flacour response the flavor and the insitu LAr EM scale. These were chose based on a study of the nuisance paramters for the fits. The results are presented in Table 4. We see that the changes has a huge impact on the values of $\frac{\chi^2}{ndf}$. A more thorough treatment of this was not done as a part of this project.

## 5.2 $\chi^2$ parabolas

To analyse and compare the fits of the individual data sets and their influence on the global or experiment specific fit we developed an Alpos task Chi2Scan, which calculates $\chi^2$ parabolas for the fits. In Figures 5, 6, 7, 8 we have included the $\chi^2$ parabolas for the global fit, the LHC data, the HERA data, and the Tevatron data, with the $\chi^2$ parabolas of their respective contributions.

## 5.3 Theory uncertainties

If we look back to the cross section definitions in (5) and (6) we see that for the determination of $\alpha_s(M_Z)$ we have got uncertainty from cross section through the fitting in Alpos. The theoretical uncertainties from the PDF's $f(x, \mu_f, \hat{\alpha_s})$ and the choice of scales in $\hat{\sigma}(\mu_r, \mu_f)$.

The uncertainty on the PDF can be seperated into two parts. One that regards just the PDF set $f(\dots)$ in use and another that regards the choice of $\alpha_s$ for the PDF.

First we deal with the uncertainty from the PDF set. In order to find the uncertainty from our PDF set, NNPDF30_nlo_as_0118 we looped through all the 100 PDF sets,

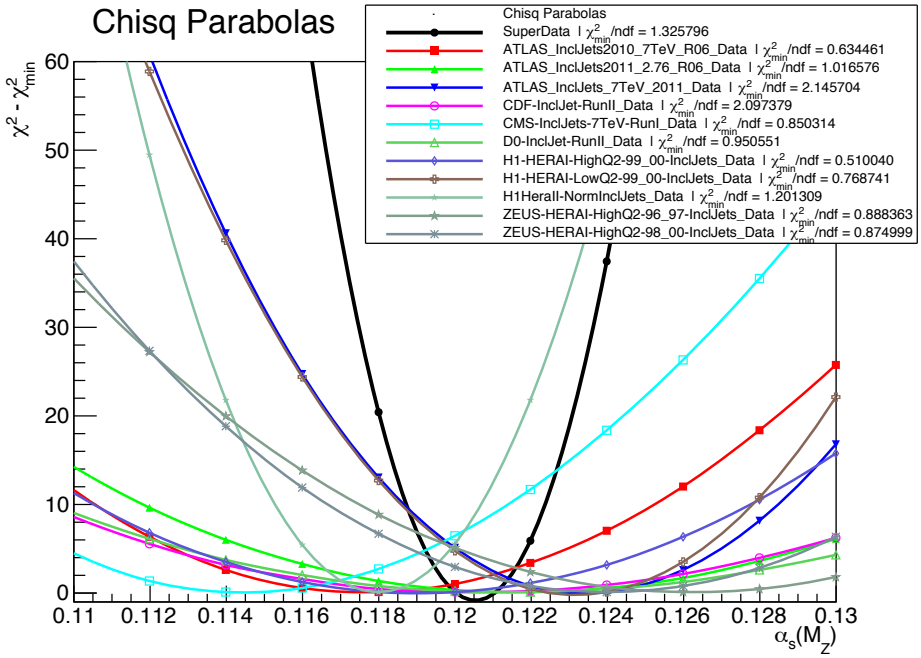


Figure 5: $\chi^2$ parabola for the global fit. SuperData represents the global fit, and the other entries are fits of the contributing data.

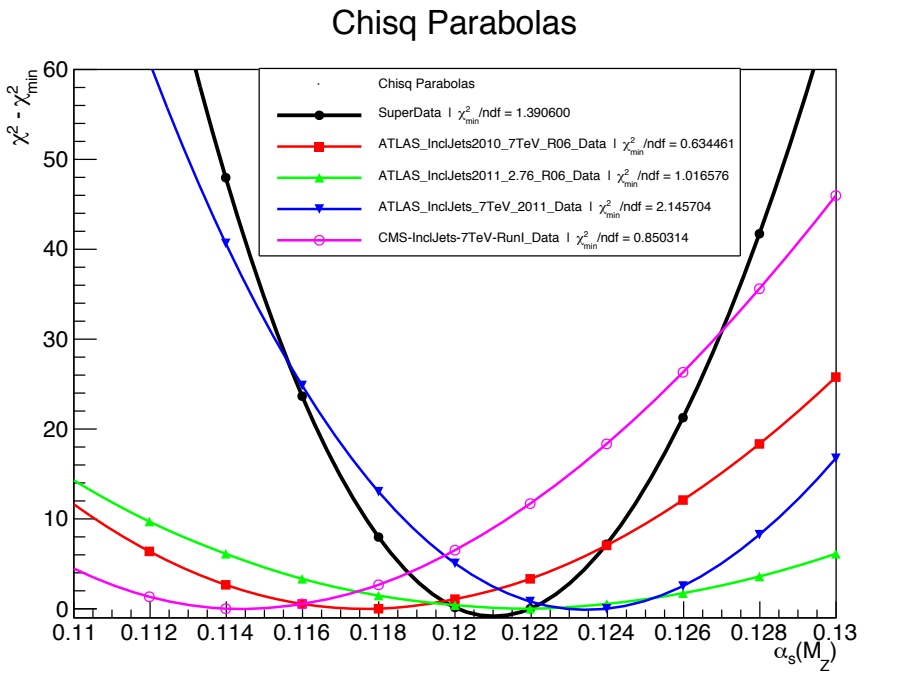


Figure 6: $\chi^2$ parabola for a fit of the LHC data. SuperData represents the overall LHC fit, and the other entries are fits of the ATLAS and CMS data.

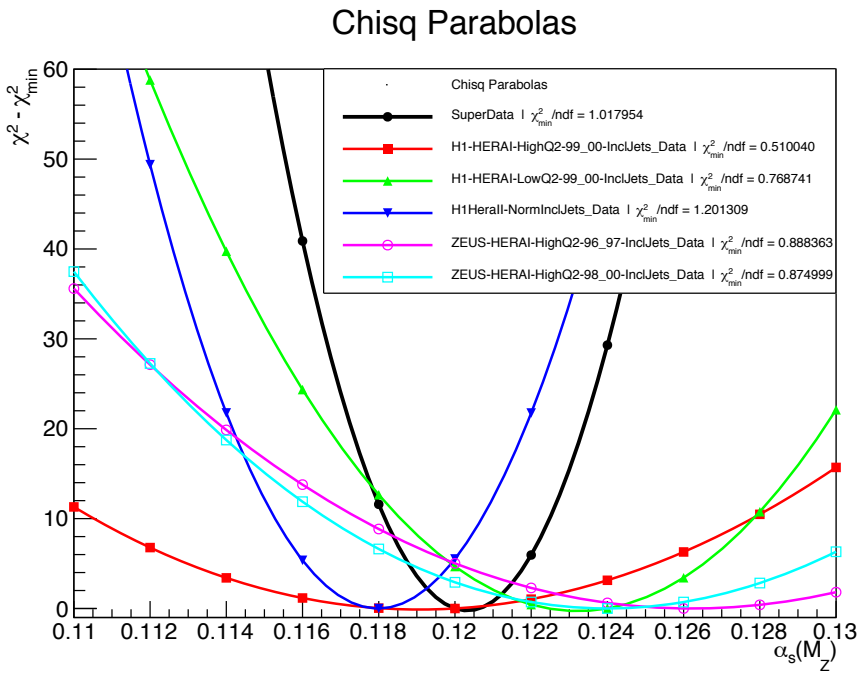


Figure 7: $\chi^2$ parabola for a fit of the HERA data. SuperData represents the overall HERA fit, and the other entries are fits of the H1 and ZEUS data.

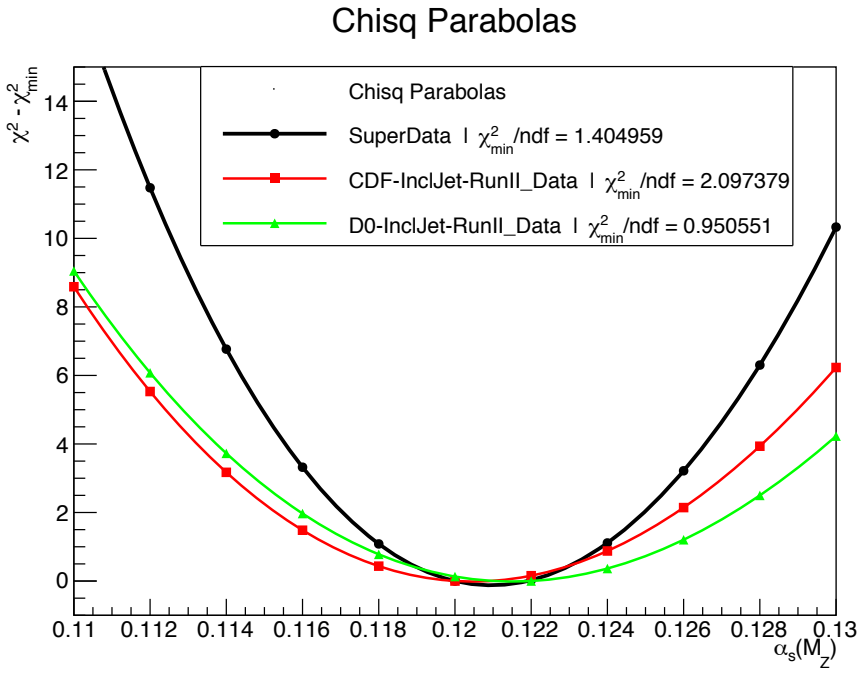


Figure 8: $\chi^2$ parabola for a fit of the Tevatron data. SuperData represents the overall Tevatron fit, and the other entries are fits of the CDF and DØ data.

which NNPDF30_nlo_as_0118 consists of, and make a fit of the $\alpha_s(M_Z)$ value, which we store in a histogram. In this study we have implemented the Alpos task PDFUncer to perform these fits. The histograms from the fits using global, HERA, LHC and Tevatron data are included in Figures 9, 10, 11, 12, and the resulting uncertainties also including individual detector data are presented in Table 5.

Next we have the uncertainty from the choice of $\alpha_s$ for the extraction of the PDF set. We have choosen a PDF set NNPDF_nlo_as_0118 which is extracted for $\alpha_s = 0.118$. From [9] we have an uncertainty on $\alpha_s$ of 0.001. To find out how this uncertainty propagates into our fit we can run fits with the PDF sets NNPDF30_nlo_as_0119 and NNPDF30_nlo_as_0117 and calculate

$$\sigma_{PDF,\hat{\alpha_s}} = \frac{1}{2}(\alpha_s^{\text{NNPDF\_0119}} - \alpha_s^{\text{NNPDF\_0117}}) \quad (10)$$

The results of this is given in Table 6

Table 5: Results of PDF uncertainty calculations

| **Data set** | $\boldsymbol{\sigma_{PDF}}$ **(RMS)** |
|---|---|
| Global | 0.00050 |
| LHC | 0.00127 |
| ATLAS | 0.00092 |
| CMS | 0.0026 |
| HERA | 0.00052 |
| H1 | 0.00048 |
| ZEUS | 0.00088 |
| Tevatron | 0.00194 |
| CDF | 0.00176 |
| D0 | 0.00230 |

Now that we have delt with the PDF specific uncertainties we move on to the scale uncertainties. In the steering file for the Alpos code we have the parameters `fastNLO.ScaleFacMuR` and `fastNLO.ScaleFacMuF` that can be used to set $\mu_R$ and $\mu_F$ for the fit. In order to find the uncertainty from the choise of scales we perform fits where we vary the scale values and compute the following formular.

First for the uncertainty for $\mu_r$:

$$\sigma^+_{\alpha_s}(c_{\mu_r}) = \left|\alpha_s(c_{\mu_r}=1, c_{\mu_f}=1) - \alpha_s(c_{\mu_r}=2, c_{\mu_f}=1)\right|$$
$$\sigma^+_{\alpha_s}(c_{\mu_r}) = \left|\alpha_s(c_{\mu_r}=1, c_{\mu_f}=1) - \alpha_s(c_{\mu_r}=0.5, c_{\mu_f}=1)\right|$$

Then for the uncertainty for $\mu_f$:

$$\sigma^+_{\alpha_s}(c_{\mu_f}) = \left|\alpha_s(c_{\mu_r}=1, c_{\mu_f}=1) - \alpha_s(c_{\mu_r}=1, c_{\mu_f}=2)\right|$$
$$\sigma^+_{\alpha_s}(c_{\mu_f}) = \left|\alpha_s(c_{\mu_r}=1, c_{\mu_f}=1) - \alpha_s(c_{\mu_r}=1, c_{\mu_f}=0.5)\right) \ ,$$

where $\alpha_s(c_{\mu_r}=a, c_{\mu_f}=b)$ indicated a fitted value with the parameter `fastNLO.ScaleFacMuR` set to $a$ and `fastNLO.ScaleFacMuF` set to $b$.

These calculations have been made for the global data as well as for the different experiments and for the individual detectors. The results are presented in Table 7.

What we immediatly can see from these uncertainties are that they are larger than the experimental uncertainties and the PDF uncertainties, especially $\sigma_{\alpha_s}(\mu_r)$. That will

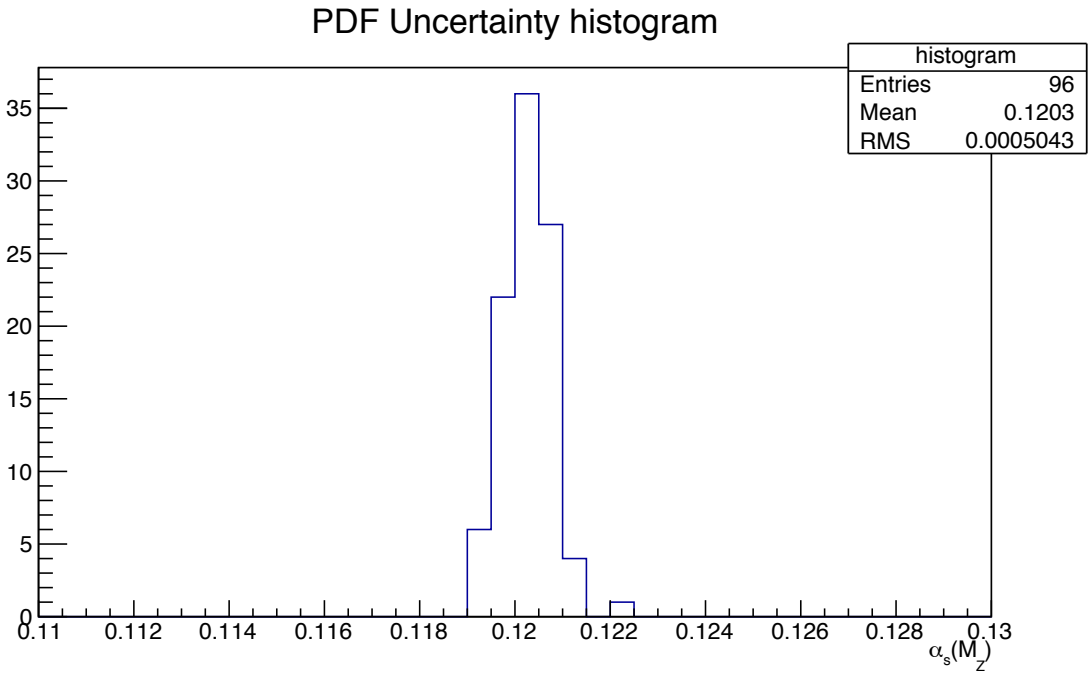


Figure 9: Histogram of global $\alpha_s(M_Z)$ fits for the PDF sets that contributes to the NNPDF30_nlo_as_0118 PDF set.

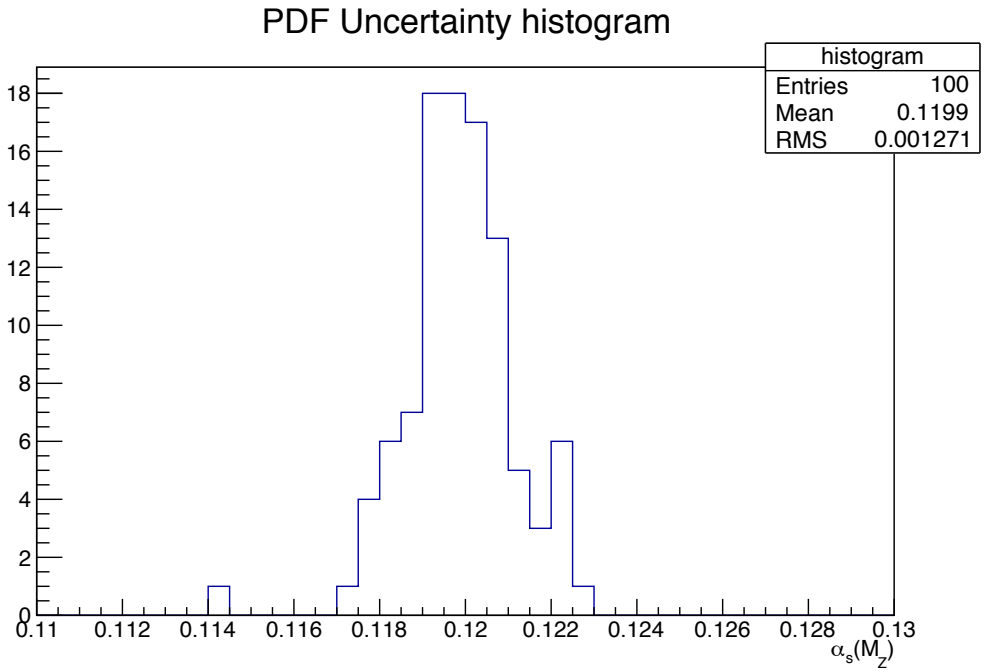


Figure 10: Histogram of LHC data $\alpha_s(M_Z)$ fits for the PDF sets that contributes to the NNPDF30_nlo_as_0118 PDF set.

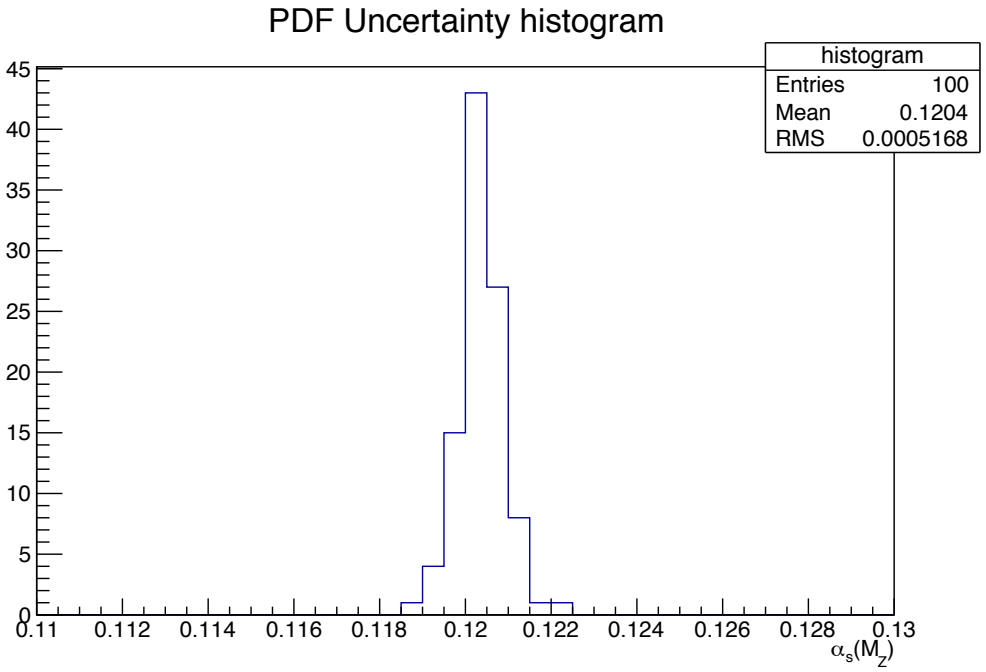


Figure 11: Histogram of HERA data $\alpha_s(M_Z)$ fits for the PDF sets that contributes to the NNPDF30_nlo_as_0118 PDF set.

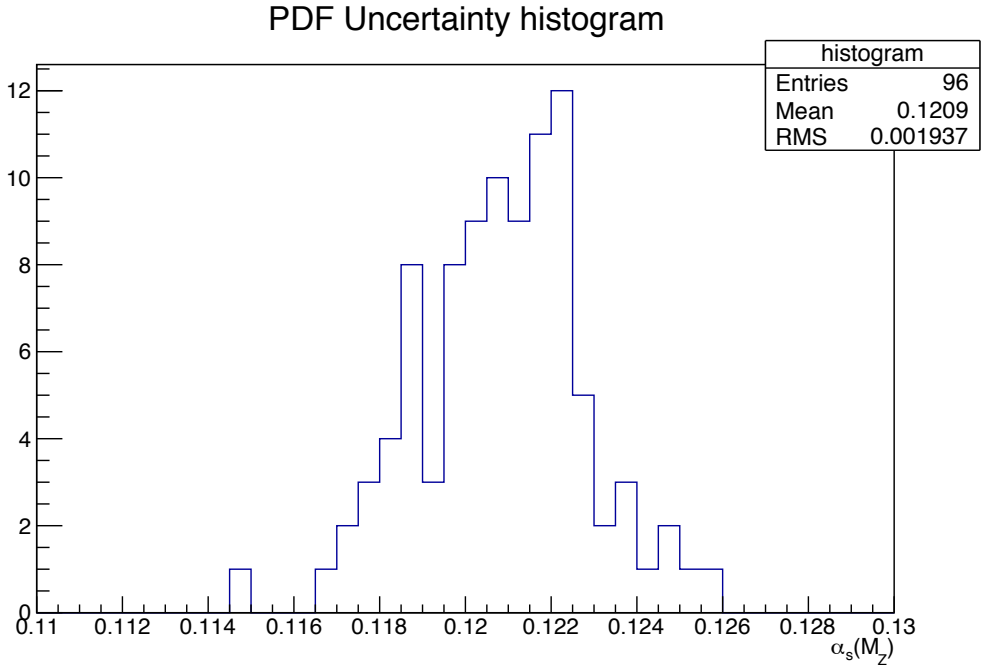


Figure 12: Histogram of Tevatron data $\alpha_s(M_Z)$ fits for the PDF sets that contributes to the NNPDF30_nlo_as_0118 PDF set.

Table 6: Results of PDF $\hat{\alpha}_s(M_Z)$ uncertainty calculations

| **Data set** | $\boldsymbol{\alpha_s^{\text{NNPDF\_0117}}}$ | $\boldsymbol{\alpha_s^{\text{NNPDF\_0117}}}$ | $\boldsymbol{\sigma_{\text{PDF},\alpha_s}}$ |
|---|---|---|---|
| Global | 0.119982 | 0.12085 | 0.000434 |
| LHC | 0.119898 | 0.120687 | 0.0003945 |
| ALTAS | 0.121697 | 0.122264 | 0.0002835 |
| CMS | 0.114704 | 0.116108 | 0.000702 |
| HERA | 0.119943 | 0.120825 | 0.000441 |
| H1 | 0.119113 | 0.120099 | 0.000493 |
| ZEUS | 0.124852 | 0.125135 | 0.0001415 |
| Tevatron | 0.121074 | 0.122177 | 0.0005515 |
| CDF | 0.120789 | 0.12164 | 0.0004255 |
| D0 | 0.121399 | 0.12281 | 0.0007055 |

Table 7: Scale uncertainties for $\mu_r$ and $\mu_f$

| **Data set** | $\boldsymbol{\sigma^+_{\alpha_s}(\mu_r)}$ | $\boldsymbol{\sigma^-_{\alpha_s}(\mu_r)}$ | $\boldsymbol{\sigma^+_{\alpha_s}(\mu_f)}$ | $\boldsymbol{\sigma^-_{\alpha_s}(\mu_f)}$ |
|---|---|---|---|---|
| Global | 0.0027 | 0.0034 | 0.00062 | 0.00157 |
| LHC | 0.0030 | 0.00146 | 0.00053 | 0.00087 |
| ALTAS | 0.0017 | 0.00170 | 0.00030 | 0.00062 |
| CMS | 0.0022 | 0.00084 | 0.00125 | 0.00177 |
| HERA | 0.0024 | 0.0039 | 0.00116 | 0.0024 |
| H1 | 0.0021 | 0.0040 | 0.00122 | 0.0028 |
| ZEUS | 0.0050 | 0.0030 | 0.00092 | 0.00076 |
| Tevatron | 0.0061 | 0.0045 | 0.00093 | 0.00144 |
| CDF | 0.0061 | 0.0038 | 0.00079 | 0.00116 |
| D0 | 0.0062 | 0.0052 | 0.00110 | 0.00177 |

probably lead to the scale uncertainty from the renormalization scale $\mu_r$ to dominate the theoretical uncertainty.

We also has uncertainties from the non-perturbative corrections, $c_{NP}$ and the electroweak corrections, $c_{EQ}$. These are not included in this study.

Now that we have calculated the different uncertainties for our fit we can combine the PDF and scale uncertainties into a theory uncertainty $\sigma_{th.}$. We do this by adding the uncertainties in quadrature. Table 8 show the theoretical uncertainties for each of the

experiments, HERA, LHC and Tevatron, as well as for the global fit.

Table 8: Theory uncertainties for data sets

| **Data set** | $\boldsymbol{\sigma_{PDF}}$ | $\boldsymbol{\sigma_{PDF,\alpha_s}}$ | $\boldsymbol{\sigma_{\alpha_s}(\mu_R)}$ | $\boldsymbol{\sigma_{\alpha_s}(\mu_F)}$ | $\boldsymbol{\sigma_{th.}}$ |
|---|---|---|---|---|---|
| LHC | $\pm 0.00127$ | $\pm 0.00040$ | $^{+0.0030}_{-0.0015}$ | $^{+0.0005}_{-0.0009}$ | $^{+0.0033}_{-0.0021}$ |
| HERA | $\pm 0.00052$ | $\pm 0.00044$ | $^{+0.0024}_{-0.0039}$ | $^{+0.0012}_{-0.0024}$ | $^{+0.0028}_{-0.0046}$ |
| Tevatron | $\pm 0.00194$ | $\pm 0.00055$ | $^{+0.0061}_{-0.0045}$ | $^{+0.0009}_{-0.0014}$ | $^{+0.0065}_{-0.0051}$ |
| Global | $\pm 0.0005$ | $\pm 0.00043$ | $^{+0.0027}_{-0.0034}$ | $^{+0.0006}_{-0.0016}$ | $^{+0.0028}_{-0.0038}$ |

The result of the global fit of the $\alpha_s(M_Z)$ with included uncertainties is:

$$\alpha_s(M_Z) = 0.12055 \ \pm 0.00055 \text{ (exp.) } ^{+0.0028}_{-0.0038} \text{ (th.)}$$

The theory uncertainty incompasses uncertainti9es from PDF, $\alpha_s$ in PDF fits, and scale uncertainties, but no uncertainties on non-perturbative corrections or electroweak effects.

In Figure 13 we have made a summary plot of the fit with the data from the different experiments as well as the global fit. Here it is also compared to the current world average $\alpha_s(M_Z) = 0.1185 \pm 0.0006$ [3]. We see from the plot that the world average is within the theoretical uncertainties of our fit. Which makes it interesting to see what result we can get if we could improve the theoretical uncertainty, which is mainly due to the scale uncertainty from the choice of renormalization scale $\mu_r$

# 6 Conclusion

We have used inclusive jet cross-section data from HERA, LHC and Tevatron experiments to perform a global fit of the fundamental QCD parameter, the strong coupling constant $\alpha_s(M_Z)$. This has been done using the theory comparison and fitting framework Alpos, which takes datafiles, theoryfiles and fitting specifications as input.

We have studied how uncertainties and correlations are handled by experiments and included in Alpos fits. Also we have reviewed different PDF sets for the fitting.

After preforming the fits for the individual experiments and for all the experiments together, we studied the quality of the fits by studying the $\chi^2$ parabolas and find the theoretical uncertainties on $\alpha_s(M_Z)$.

The result for the fit is $\alpha_s(M_z) = 0.12055 \pm 0.00055$ (exp.) $^{+0.0028}_{-0.0038}$ (th.), which is cosistent with the current world average of $\alpha_s(M_Z) = 0.1185 \pm 0.0006$ [3].

Further work could be to try to improve the theoretical uncertainty. This could be done by using better PDF sets for the fitting or study how the choice of PDF sets and scale parameters affect the fitted values.

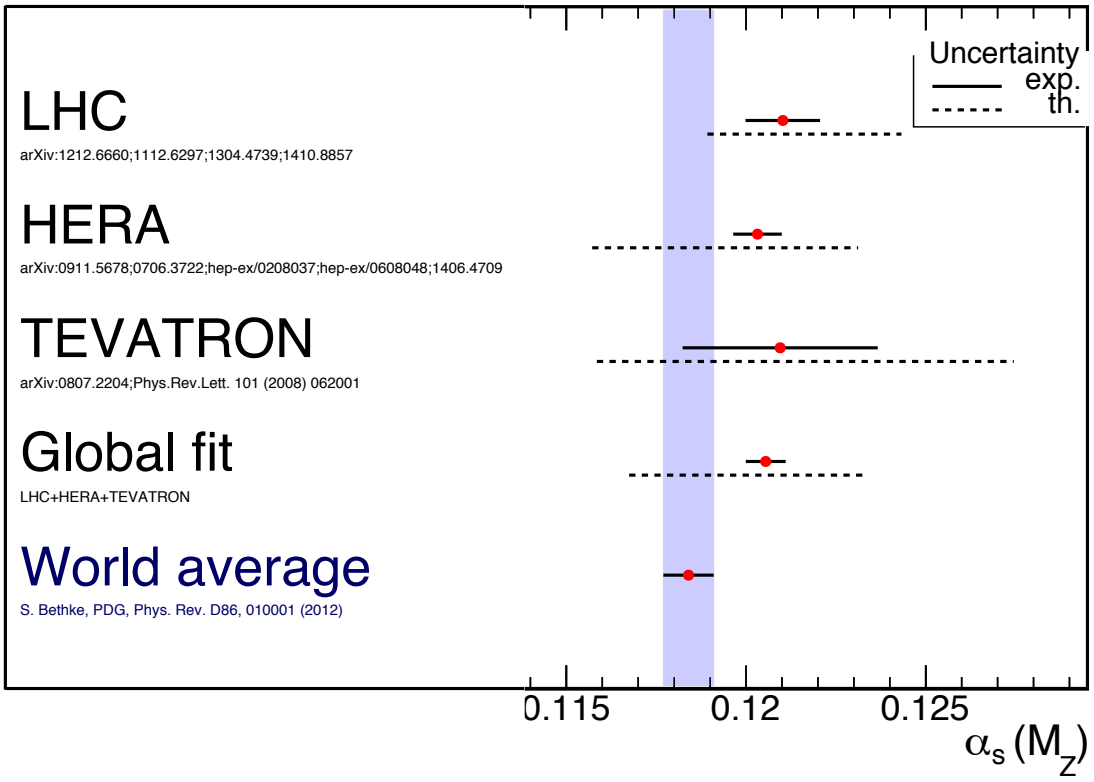


Figure 13: Summary plot for $\alpha_s(M_Z)$ fits. Blue field marks current world average of $\alpha_s(M_Z)$.

# 7 Acknowledgements

I would like to thank my supervisors, Daniel Britzger and Hayk Pirumov, for giving me the project and for help and discussions on the topic. I would also thank my office mate, Daniel Reichelt, who was working on a similar topic and under the same supervisors as me. It was great beeing a part of the ATLAS group at DESY, the ice cream fridays were awesome. A large thanks to Olaf Behnke and the DESY summer student program organizing team for making everything run smoothly. Last but least I want to thank my friends in Ausgang, I feel privliged to be included in this exclusive clique.

Table 9: Output for ATLAS 2011 7 TeV data with changes in correlations

| **Experiment** | **Process** | $\sqrt{s}$ | **Integrated_Luminosity** | **pT_range** | **y_range** | **Q2_range** | **Reference** |
|---|---|---|---|---|---|---|---|
| H1-HERAI-LowQ2-99/00 | DIS(ep) | 319(GeV) | 43.5 $pb^{-1}$ | 5-80 GeV | 0.2-0.7 | 5-100 $GeV^2$ | [10] |
| H1-HERAI-HighQ2-99/00 | DIS(ep) | 319(GeV) | 65.4 $pb^{-1}$ | 7-50 GeV | 0.2-0.7 | 150-15000 $GeV^2$ | [11] |
| ZEUS-HERAI-HighQ2-96/97 | DIS(ep) | 300(GeV) | 38.6 $pb^{-1}$ | 8-100 GeV | 0.2-0.7 | 125-$10^5$ $GeV^2$ | [12] |
| ZEUS-HERAI-HighQ2-98/00 | DIS(ep) | 318(GeV) | 82.0 $pb^{-1}$ | 8-100 GeV | 0.2-0.7 | 125-$10^5$ $GeV^2$ | [13] |
| H1HeraII-NormInclJets | DIS(ep) | 319(GeV) | 351.0$pb^{-1}$ | 7-50 GeV | 0.2-0.7 | 150-15000 $GeV^2$ | [14] |
| CDF-InclJet-RunII | ppbar | 1.96(TeV) | 1.13 $fb^{-1}$ | 62-200 GeV | 0.1-0.7 | | [15] |
| D0-InclJet-RunII | ppbar | 1.96(TeV) | 0.70 $fb^{-1}$ | 50-600 GeV | 0.0-2.4 | | [16] |
| CMS-InclJets-7TeV-RunI | pp | 7(TeV) | 5.0 $fb^{-1}$ | 114-2116 GeV | 0.0-2.5 | | [17] |
| ATLAS_InclJets2010_7TeV_R06 | pp | 7(TeV) | 37.0 $pb^{-1}$ | 20-1500 GeV | 0.0-4.4 | | [18] |
| ATLAS_InclJets2011_2.76_R06 | pp | 2.76(TeV) | 0.20 $pb^{-1}$ | 20-430 GeV | 0.0-4.4 | | [19] |
| ATLAS_InclJets_7TeV_2011 | pp | 7(TeV) | 4.5 $fb^{-1}$ | 100-2000 GeV | 0.0-3.0 | | [20] |

# References


[1] *G. Zweig, "An SU(3) model for strong interaction symmetry and its breaking*, CERN-TH-401 (1964)

[2] *H. Fritzsch et al., "Advantages of the Color Octet Gluon Picture"*, Phys. Rev. 96 (1973) 191-195.

[3] *K.A. Olive et al.* (Particle Data Group), *9. Quantum Chromodynamics*, Chin. Phys. C, 38, 090001 (2014)

[4] *K.A. Olive et al.* (Particle Data Group), *38. Statistics*, Chin. Phys. C, 38, 090001 (2014)

[5] *M. Wobisch et al.* (The fastNLO Collaboration), *Theory-Data Comparisons for Jet Measurements in Hadron-Induced Processes*, DESY 11-150 (arXiv:1109.1310v1) 6 Sep 2011

[6] *S. Dulat et al., The CT14 Global Analysis of Quantum Chromodynamics*, (arXiv:1506.07443v2) 2 Aug 2015

[7] *L.A. Harland-Lang, Parton distributions in the LHC era: MMHT 2014 PDFs*, (arXiv:1412.3989v2) 14 May 2015

[8] The NNPDF Collaboration, *Parton distributions with LHC data*, (arXiv:1207.1303v2) 26 Sep 2012

[9] The NNPDF Collaboration, *Parton distributions for the LHC Run II*, (arXiv:1410.8849) 4 May 2015

[10] H1 Collaboration, *Jet Production in ep Collisions at Low $Q^2$ and Determination of $\alpha_s$*, DESY 09-162 (arXiv:0911.5678v2) 23 Feb 2010

[11] H1 Collaboration, *Measurement of Inclusive Jet Production in Deep-Inelastic Scattering at High $Q^2$ and Determination of the Strong Coupling*, DESY 07-073 (arXiv:0706.3722v2) 3 Jul 2007

[12] ZEUS Collaboration, *Inclusive jet cross sections in the Breit frame in neutral current deep inelastic scattering at HERA and determination of $\alpha_s$*, DESY 02-112 (arXiv:hep-ex/0208037v1) 22 Aug 2002

[13] ZEUS Collaboration, *Inclusive-jet and dijet cross sections in deep inelastic scattering at HERA*, DESY 06-128 (arXiv:hep-ex/0608048v2) 25 Sep 2006

[14] H1 Collaboration, *Measurement of Multijet Production in ep Collisions at High $Q^2$ and Determination of the Strong Coupling $\alpha_s$*, DESY 14-089 (arXiv:1406.4709v2) 6 Oct 2014

[15] CDF Collaboration, *Measurement of the Inclusive Jet Cross Section at the Fermilab Tevatron $p\bar{p}$ Collider Using a Cone-Based Jet Algorithm*, (arXiv:0807.2204v4) 27 May 2009

[16] D0 Collaboration, *Measurement of the Inclusive Jet Cross Section in pp Collisions at* $\sqrt{s} = 1.96$ *TeV*, (PRL 101,062001) 8 August 2009

[17] The CMS Collaboration, *Measurements of differential jet cross sections in proton-proton collisions at* $\sqrt{s} = 7$ *TeV with the CMS detector*, CERN-PH-EP/2012-343 (arXiv:1212.6660v2) 4 Jun 2013

[18] The ATLAS Collaboration, *Measurement of inclusive jet and dijet production in pp collisions at* $\sqrt{s} = 7$ *TeV using the ATLAS detector*, CERN-PH-EP-2011-192 (arXiv:1112.6297v2) 16 Apr 2012

[19] The ATLAS Collaboration, *Measurement of the inclusive jet cross-section in pp collisions at* $\sqrt{s} = 2.76$ *TeV and comparison to the inclusive jet cross-section at* $\sqrt{s} = 7$ *TeV using the ATLAS detector*, CERN-PH-EP-2013-036 (arXiv:1304.4739v2) 9 Oct 2013

[20] The ATLAS Collaboration, *Measurement of the inclusive jet cross-section in protonproton collisions at* $\sqrt{s} = 7$ *TeV using* $4.5fb^1$ *of data with the ATLAS detector*, CERN-PH-EP-2014-155 (arXiv:1410.8857v2) 2 Apr 2015